We are IntechOpen, the world's leading publisher of Open Access books Built by scientists, for scientists

6,900
Open access books available

185,000
International authors and editors

200M
Downloads

154
Countries delivered to

Our authors are among the

TOP 1%
most cited scientists

12.2%
Contributors from top 500 universities

CLARIVATE ANALYTICS
BOOK CITATION INDEX
INDEXED

WEB OF SCIENCE™

Selection of our books indexed in the Book Citation Index
in Web of Science™ Core Collection (BKCI)

Interested in publishing with us?
Contact book.department@intechopen.com

Numbers displayed above are based on latest data collected.
For more information visit www.intechopen.com

Statistical Physics Modeling of Disordered Metallic Alloys

Ryan P. Cress and Yong W. Kim

Abstract

The great majority of metallic alloys in use are disordered. The material property of a disordered alloy changes on exposure to thermal, chemical, or mechanical forcing; the changes are often irreversible. We present a new first principle method for modeling disordered metallic alloys suitable for predicting how the morphology, strength, and transport property would evolve under arbitrary forcing conditions. Such a predictive capability is critically important in designing new alloys for applications, such as in new-generation fission and fusion reactors, where unrelenting harsh thermal loading conditions exist. The protocol is developed for constructing a coarse-grained model that can be specialized for the evolution of thermophysical properties of an arbitrary disordered alloy under thermal, stress, nuclear, or chemical forcing scenarios. We model a disordered binary alloy as a randomly close-packed (RCP) assembly of constituent atoms at given composition. As such, a disordered alloy specimen is an admixture of nanocrystallites and glassy matter. For the present purpose, we first assert that interatomic interactions are by repulsion only, but the contributions from the attractive part of the interaction are restored by treating the nanocrystallites as nanoscale pieces of a single crystalline solid composed of the same constituent atoms. Implementation of the protocol is discussed for heating of disordered metals, and results are compared to the known melting point data.

Keywords: nanocrystallite size distribution, glassy state atoms, simulated alloy specimen, thermal forcing, melting point

1. Introduction

Under thermal, mechanical, or chemical forcing, disordered metallic alloy specimens may change in their thermophysical properties, such as thermal diffusivity, electrical resistivity,

spectral emissivity, and many other properties. The degree to which such modifications are materialized depends on both the intensity and duration of the forcing. In the case of a thermal forcing, the temperature serves as the control parameter of forcing in reference to the specimen's intrinsic threshold properties, such as the melting point. The modification has serious consequences in utilization of metallic alloys in high-temperature and high-stress processes. Examples are found in nuclear reactors, chemical reactors, pyrometallurgical processes, and others. Thermophysical properties of alloys drift away from the design values, compromising the performance metrics as well as even leading to material failures.

The questions are why and how such a forcing modifies the material's basic thermophysical properties. Two characteristic features highlight alloy modifications due to thermal forcing: one, enrichment of the more mobile atoms near the alloy surface, which has been observed in direct Measurement; and two, the morphological transformation as quantified in terms of the nanocrystallite size distribution [1, 2]. Both of the features influence the transport of mass, momentum, and energy because the exact details of the pathways for transport of flux quanta across a surface are determined by them. The latter feature is a precursor to alloy melting, and we show that the associated morphological transformation can be theoretically treated. This theoretical treatment will lead to a better understanding of the changing factors that influence the thermophysical properties of the alloy.

We focus on identifying the basic physical mechanisms that affect thermophysical properties of simple metallic alloys and incorporating their coarse-grained formulations, or their simplest representations, into the alloy model. The goal is to render the construction of a realistic model of any arbitrary disordered alloy easy and simple. We hypothesize that the changes in the alloy's thermophysical properties are mediated by the changes in the size distribution function of nanocrystallites due to re-equilibration of nanocrystallites in size distribution at elevated temperatures. Transport of excitations through a thermally forced disordered alloy specimen would involve two different material media, crystalline versus glassy, whose physical sizes have been modified due to thermal forcing, and transmission of excitations across the interfaces between them has also been modified. The rates of excitation transport through the specimen would thus be changed as a result of the modifications of the distribution function of the nanocrystallites. It has been shown for a number of different alloys that the thermal forcing results in changes of the specimen's elemental composition profile as a function of depth from the surface, distinctly different from the bulk composition [3–5].

The theoretical insight into the state of the atomistic structure of a disordered binary alloy can help quantify the contributions from the structural properties of the alloy specimen to the transport of thermal excitations through the alloy. After setting up the theoretical model of how this structure would change as a function of temperature, we can proceed with predicting how the thermal transport properties would be affected by the morphological changes and move on to mapping out the changing thermophysical properties. The theoretical prediction of how such modifications would materialize will go a long way toward developing new materials and forecasting the modes of structural failures in existing materials.

Available experimental data on the thermal conductivity of solids vary widely. This is in part due to difficulties in making accurate measurement of the thermal conductivities of solids and

in part due to problems in physical and chemical characterization of the test specimens of such solids. In the case of disordered binary alloys, these complications lead to serious gaps in experimental data in conflict with the thermodynamic property data that are available. Experimental uncertainties in measurement can arise from many different sources, including poor sensitivity of measuring instruments and sensors, specimen contamination, stray heat flows that are unaccounted for, and incorrect form factors of the test specimens. Perhaps, the most serious problem is in the indeterminate nature of the alloy composition itself, as experimentalists are often unsure of the elemental composition of their specimens [6]. More recent studies on the properties of binary alloys have focused on binary alloys as polycrystalline materials. In the context of binary alloys, the polycrystalline model suggests crystallite grains separated by grain boundaries. In such a material, the physics of the interfaces between nanocrystallites tend to dominate the transport properties of the alloy [7]. Because of the high density of grain boundaries, recent efforts have focused on controlling of the formation of grain boundaries in order to produce more stable binary alloys for high temperature processes [8].

2. Modeling of disordered alloys as a RCP assembly of constituent atoms

Since the introduction of complex metallic alloys as a material, the question has been on how the atoms in such metals arranged themselves. In this context, Bernal first imagined the alloy as a random assembly of hard spheres [9]. The radii of the spheres would correspond to the atomic radii of the constituent atoms within the alloy. Studying of the packing of spheres has a long history because of its ability to serve as a simple but useful model for a variety of physical systems [10]. The molecular nature of fluids and glasses has also enjoyed the physical visualization by hard sphere packing [11, 12]. Dense packing of hard spheres is generally separated into three subclasses: ordered close packing, random close packing, and random loose packing. Ordered close packing in three dimensions reveals periodic symmetry arising from a unit cell structure and accounts for the highest density of hard spheres [13]. Random close packing has historically been studied experimentally by filling a container with hard spheres at random and shaking the container to achieve a maximum random packing [14]. Random loose packing is the result of not shaking the container creating a less dense version of random close packing [15].

Berryman formalized the concept of random close packing (RCP). In order to have a randomly close-packed structure, it was required that all spheres be arranged at random and that the structure filled a volume at maximum density where all spheres are in contact with more than one other sphere [16]. Berryman also reported a packing fraction of 0.64 on average for RCP in three dimensions. He found that random loose packing is in some sense less fundamental than the concept of random close packing, as the definition of random loose packing requires a minimum density below which the configurations of the structure are unstable and therefore not "packed." As packing fraction increases, the phase of the matter being simulated changes. The lowest branch corresponds to the liquid phase, a packing fraction of around 0.49 corresponds to the freezing point. Packing fractions greater than 0.49 correspond to a solid phase. We are interested in the metastable branch equivalent to a mixed phase of disordered glassy

arrangements and ordered nanocrystallites. This branch will provide a foundation for the structure of disordered alloys. The metastable branch is an extension of the liquid phase and extends to the random close-packed state [17].
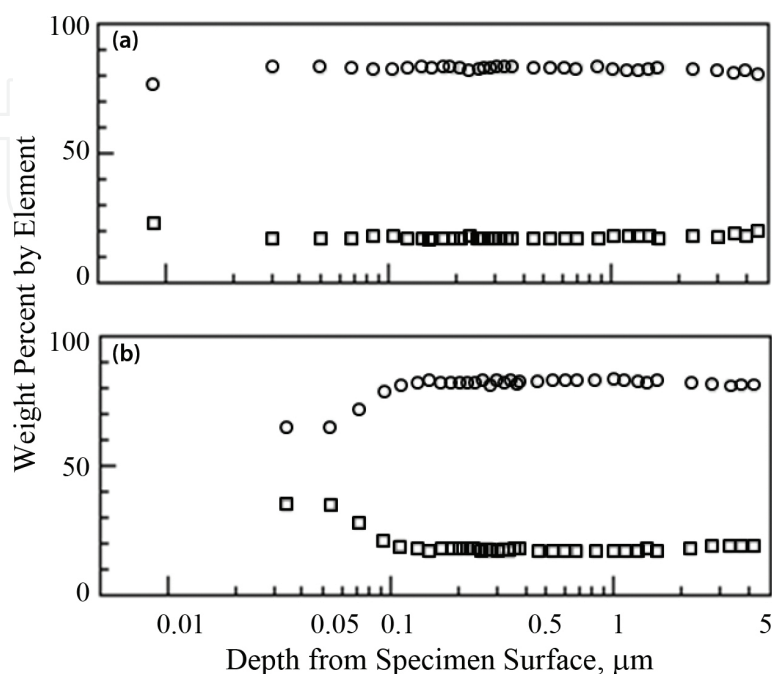
Figure 1. Measured alloy composition of a 80W%Ni-20W%Cr Nichrome ribbon specimen by element (nickel in circles and chromium in squares) as a function of depth from the surface by means of the method of laser-produced plasma spectroscopy: (a) fresh specimen at room temperature before thermal forcing (top); and (b) fresh specimen cooled to room temperature after a 15-hour heating in vacuum at 1100 K (bottom) [1–5].

The pivotal experiment in developing the structural model of disordered binary alloys was the study of alloy composition as a function of depth from the surface. **Figure 1** shows the measured elemental composition of a Nichrome specimen by the method of laser-produced plasma (LPP) plume spectroscopy [5]. The laser pulse heats the surface, launching a thermal diffusion front heading into the bulk. As the power density is increased, ablation of surface atoms takes place, initiating a delayed ablation front that is also directed into the bulk. When the power density exceeds about 1×10^{10} W/cm^2, these two fronts travel at the same velocity in lock step and the atomic plume from the target surface becomes a very high density plasma plume that is in local thermodynamic equilibrium. As such, the elemental composition of the plasma plume becomes representative of the alloy specimen in elemental composition. In its afterglow regime of the plasma, it is possible to make quantitative measurement of the elemental populations as a function of depth. **Figure 1** shows the two sets of measurement for the two specimens taken out of a same batch of Nichrome alloy, one fresh specimen at room temperature and another fresh specimen at room temperature but after 15 hours of heating in vacuum at 1100 K. We see that the thermal forcing has modified the near-surface composition profile dramatically. The chromium enrichment at the specimen surface means two aspects in their transport: one, the availability of excess mobile atoms, by virtue of thermal forcing at elevated temperature; and two, preferential drift of chromium atoms over nickel atoms toward

the surface due to their mass difference, in the presence of the Coulomb force between an atom and its image charges at the specimen surface.

The key question here is where the sources of excess mobile atoms are. We postulate that the excess mobile particles arise from dissociation of nanocrystallites within the disordered alloy specimen under thermal forcing at elevated temperatures. The dissociation adds to the populations of glassy state atoms, and such atoms are less tightly bound to glassy state clusters than to nanocrystallites. Both chromium and nickel atoms drift toward the surface but by virtue of its slightly smaller mass, enrichment of chromium atoms results at the surface. The thickness of the chromium-enriched region near the surface grows in proportion to the length of the time of thermal forcing and the forcing temperature [1].

## 3. Nanocrystallite size distribution

The order within an RCP model can be quantified by means of the degree of crystallinity in the structure. The degree of crystallinity is the probability that an atom in the structure is part of nanocrystallites rather than being part of glassy state clusters. The basic building block of a nanocrystallite in three dimensions is a tetrahedron composed of four spheres [18]. To define the structure of a disordered binary alloy specimen, we proceed first to determine the distribution of nanocrystallites by size in two dimensions. The distribution function in two dimensions is then transformed into three dimensions. The normalization constant of the distribution function is found by requiring that the integral of the distribution over size can be equated to the degree of crystallinity multiplied by the total number of atoms in the specimen. The nanocrystallite size distribution in three dimensions is found by transforming the distribution in two dimensions into one in three dimensions.

As it turns out, the degree of crystallinity of a structure has a strong dependence on alloy composition fraction. The structure we use as the basis for the arrangement of atoms in a binary alloy is first measured in two dimensions using a simulated two-dimensional (2D) assembly of spheres. Alloys of different compositions are constructed by mixing the spheres of two different diameters. Here, we assert that the primary physics that controls the size of crystalline assembly is the repulsive part of the inter-particle interaction potential, ignoring the attractive part at this stage. The attractive interaction plays significant roles in capturing the symmetry property of the alloy's nanocrystallites. This is fully realized when we compose the theoretical model of the disordered alloy in atomic dimensions; we make use of the known crystalline structure of the alloy according to the established solid-state database of the particular crystalline assembly of atoms as a disordered solid specimen. More details will be given when we present the specific example of $AuCu_3$.

The simulated assembly of the hard spheres in two dimensions is randomly reinitialized by random close packing and analyzed for nanocrystallites by means of digital photography. This sequence of measurement for characterization of disorder in an alloy specimen is repeated many times to find a statistically stable nanocrystallite size distribution. Two different size spheres were mixed into a single layer within a rectangular 2D container with a transparent

base, according to given alloy composition. The mixture is randomized each time by tilting the baseplate of the assembly about the horizontal plane back and forth for five times. A high-resolution digital image is taken of the assembly under diffuse illumination from below after each randomization routine. The images are analyzed for determination of particle positions and identify the nanocrystallites. We identify a nanocrystallite as an assembly of spheres, where all constituent spheres of the nanocrystallite are in contact with at least two other spheres. This basic rule is applied throughout to identify nanocrystallites of different sizes at each alloy composition.
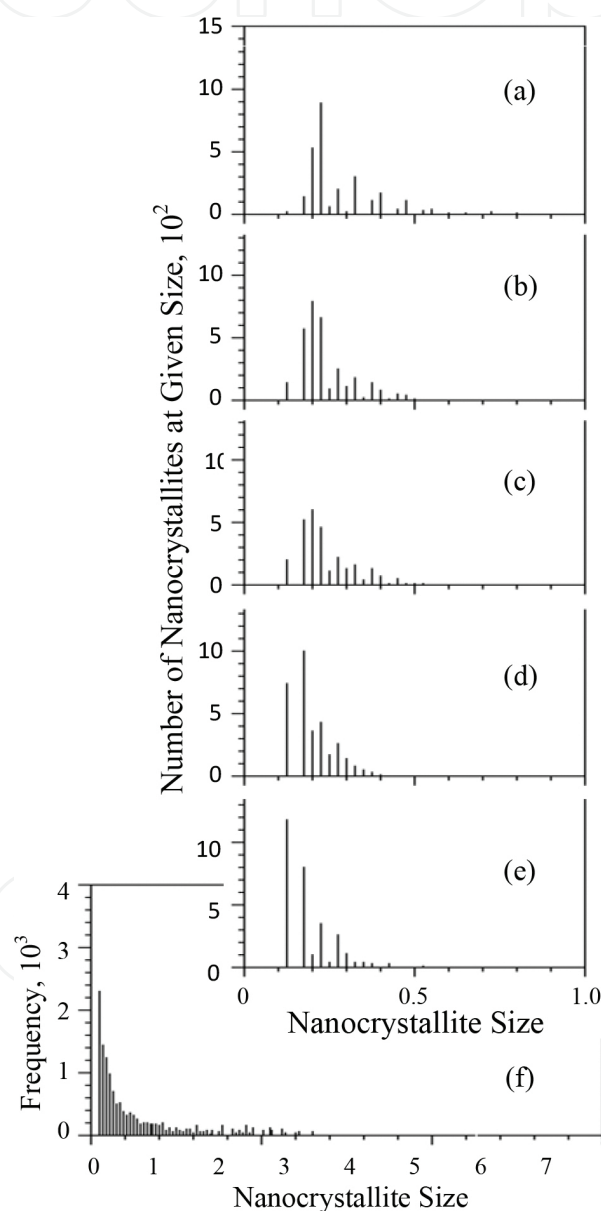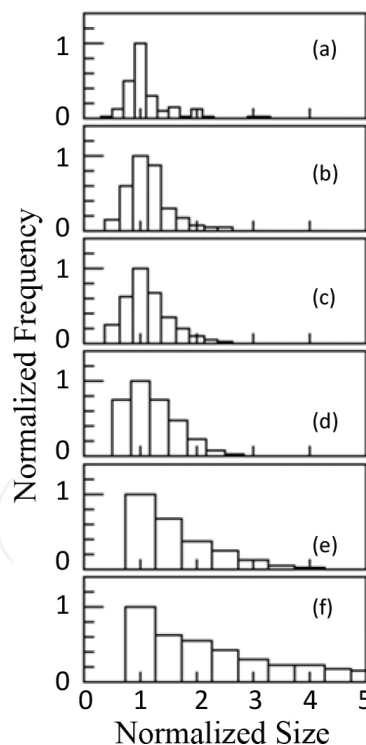

Figure 2. The frequency of occurrence of nanocrystallites as a function of nanocrystallite size for six different compositions: (a) 20W%Small:80%Large; (b) 40%S:60%L; (c)50%S:50%L; (d) 75%S:25%L; (e) 90%S:10%L; and (f) 100%S:0%L. The nanocrystallite size is given in terms of the radius of the smallest circular area into which all particles of the nanocrystallite can be fit in.

A nanocrystallite of a certain number of spheres can be made up of many different combinations of small and large spheres. For simplicity, the nanocrystallite size was identified by an effective radius, which is determined by weighted mean value of radii of spheres making up a nanocrystallite at given alloy composition. Experimental results are shown in **Figure 2**. They show a strong composition dependence on both the degree of crystallinity and the nanocrystallite size distribution.

4. Monte-Carlo simulation of disordered RCP alloys

Direct measurement of the nanocrystallite size distribution is an extremely time-consuming exercise. In order to help ease the process of applying the alloy modeling process, we have developed a Monte-Carlo code technique for simulating a disordered RCP binary alloy specimen for any given alloy composition. An ensemble of these numerically simulated alloy specimens is analyzed to obtain the nanocrystallite size distribution function for the alloy that is comparable to the measurement of the type shown in **Figure 2**. The Monte-Carlo code is structured to reproduce the suite of the measured nanocrystallite size distribution functions at six different alloy compositions.


Figure 3. The normalized nanocrystallite size distribution function is shown for six different alloy compositions. The normalized frequency of occurrence is relative to the maximal value, and the normalized nanocrystallite size is normalized with respect to the maximal radius, i.e., the most populous size in two dimensions. The measured degree of crystallinity γ, which is defined as the probability that an atom is part of nanocrystallites in the specimen, is also tabulated: (a) 20W%Small:80%Large, $\gamma = 0.456$; (b) 40%S:60%L, $\gamma = 0.479$; (c) 50%S:50%L, $\gamma = 0.307$; (d) 75%S:25%L, $\gamma = 0.316$; (e) 90%S:10%L, $\gamma = 0.486$; and (f) 100%S:0%L, $\gamma = 0.640$.

We have found that the Monte-Carlo code must be subjected to two basic rules as follows. The alloy building process begins with three-particle crystallite as a seed in two dimensions or four-particle crystallite in three dimensions. The next particle is selected randomly according to given alloy composition. In two dimensions, the selected particle is placed next to the seed nanocrystallite. When the particle is placed in one of the three crystal points the seed crystallite grows in size by one. The crystal points are located between two particles that are in contact with particles of the nanocrystallite. When it is placed at any other point, the glassy state medium grows larger by one. After many runs of the numerical simulation, we have compiled the probability for placing the new particle into a crystal point in such a way that the measured nanocrystallite size distribution functions are replicated. We have found that the probability that replicates the nanocrystallite size distribution functions of **Figure 3** is influenced by the degree of crystallinity of the specimen. But its dependence on alloy composition is found to be very weak and thus ignored.

Rule one is that each new particle introduced into the alloy specimen being constructed be selected according to the probability of being placed into a crystal point, as shown in **Figure 4**. The probabilities that are most successfully replicating the measurements of **Figure 3** are shown as a function of the degree of crystallinity.
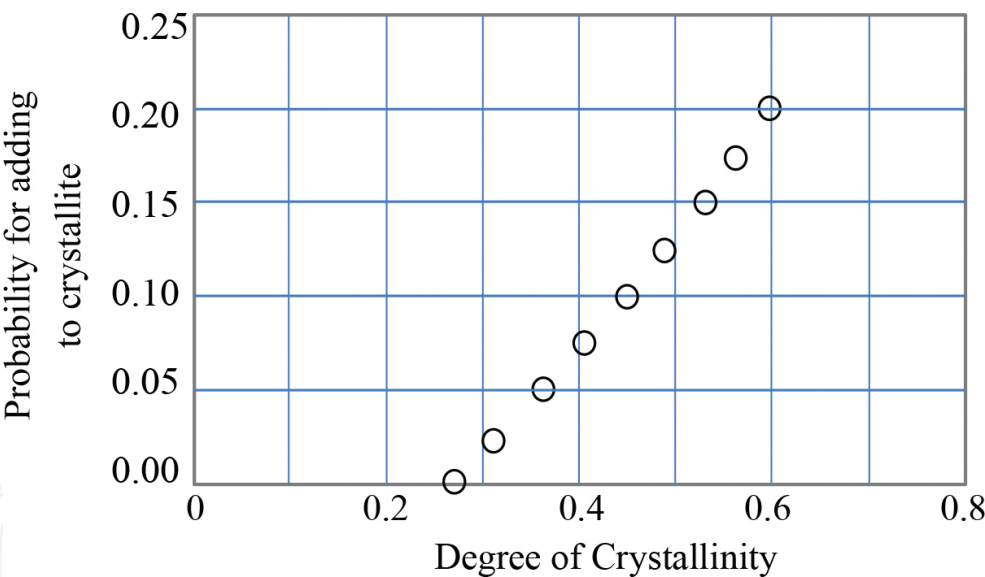
Figure 4. The probability that a new particle introduced into the numerically simulated alloy medium is placed at one of the crystal points of the nanocrystallite under numerical construction.

As one proceeds with construction of an alloy specimen of given composition by numerical simulation, the outer edges of the specimen invariably develop fingered growth fronts. These patterns appear entirely stochastically, and if left unattended, the simulated specimen becomes filled with numerous large-scale defects of open voids. Rule two is to choke off the growth of such large-scale defects by inserting a particle as soon as the gap between two nearest neighbor particles becomes equal to, or larger than, the diameter of the smallest particles in the pool of particles. An example of a numerically simulated monodisperse alloy is shown in **Figure 5**.
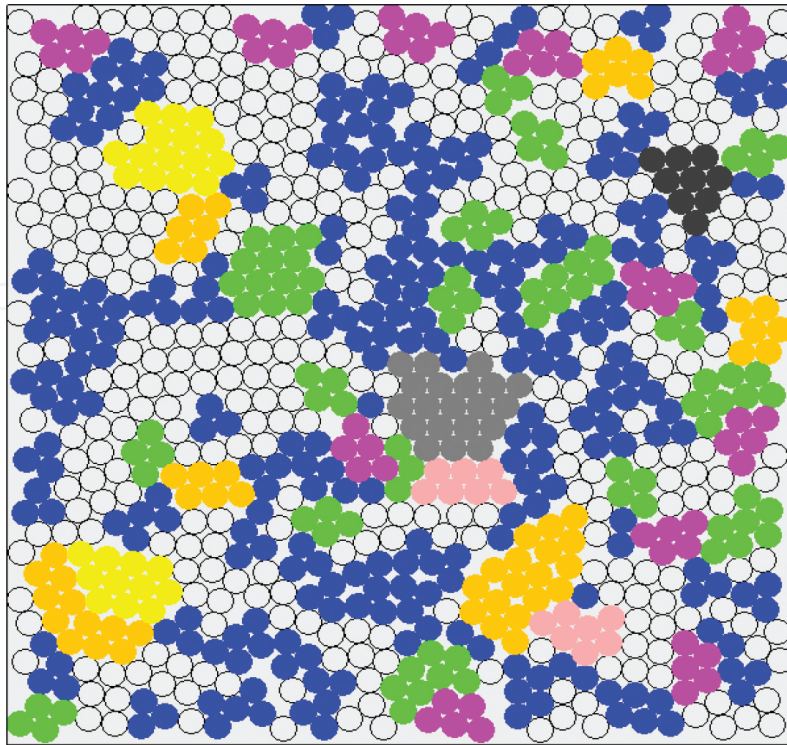
Figure 5. A sample specimen of a disordered alloy as generated by Monte Carlo code simulation.

The key data such as the nanocrystallite size distribution function can be extracted from the simulated specimens of the type shown in **Figure 5**. The simulation is repeated for a large number of times to conduct "the experiment." It is also conceivable to generalize the procedure to acquire "the experimental data" in three dimensions by simulating the alloy specimens in three dimensions according to the same rules of alloy construction that have been invoked for the construction in two dimensions.

5. Dissociation equilibrium of nanocrystallites under thermal forcing

In the present approach, a disordered alloy specimen is modeled as a random mixture of nanocrystallites and glassy atoms at room temperature and constrained by the degree of crystallinity at given alloy composition. When the specimen is forced at an elevated tempera-ture, the constituent nanocrystallites and glassy state atoms undergo excitations in the form of phonons, positional displacements, and structural transformations within the bounds of Maxwell-Boltzmann statistics. At some point in the forcing at a fixed temperature, small movements of the constituent glassy state atoms and nanocrystallites can result in fluctuations in the mass density of the specimen. As the temperature is raised, the rates of these excitations increase to the extent that the size distribution of nanocrystallites is bound to undergo significant changes. This means that thermal dissociation of atoms from the nanocrystallites within the medium takes place into the populations of glassy state atoms. Such inelastic

processes require energies to overcome the activation energy each host structure demands of constituent atoms within the nanocrystallites.

This general coarse-grained physical picture has been examined for simulated disordered specimens in two dimensions by means of a laboratory experimental set-up. An alloy specimen is simulated in two dimensions within a 2D specimen cell, consisting of a transparent conducting baseplate bounded by a rectangular aluminum frame resting on it. The specimen cell is filled with steel spheres and is driven by two mutually orthogonal linear drive motors under computer control. Two independent stepping motors are used for this purpose. Each motor is driven chaotically according to a sequence of random numbers, which are delta-autocorrelated, i.e., the successive displacements of the sequence remain uncorrelated. The operation of the set-up has been tuned such that the distribution of particle velocities in the cell obeys the Maxwell-Boltzmann statistics exactly. When the amplitude of the stepper displacements is increased by a constant factor, the Gaussian velocity profile has been found to broaden proportionately. We have thus succeeded in producing a "mechanical oven" in which thermal forcing can be effected at different "temperatures" on the simulated alloy specimens.

The response of the specimens with 2D RCP structures to thermal forcing in the mechanical oven experiment has been investigated, and this was described in previous work [5]. Observations from a series of experiments with real alloy specimens have been viewed in the light of the simulated thermal forcing experiment. The conclusions have formed the solid basis of the microscopic physical processes that take place within each alloy specimen. What was seen in the simulated thermal forcing experiment was that the degree of crystallinity of the RCP structure decreased as a function of effective temperature due to dissociation of nanocrystallites within the specimen at elevated temperature.

Thus, we begin first principle modeling of thermal dissociation of nanocrystallites by means of the law of mass action [19]. At room temperature, the structure of a disordered alloy specimen consists a population of nanocrystallites having a certain size distribution function suspended in the sea of glassy-state atoms. The exact functional form of the size distribution is controlled by alloy composition, and so is the degree of crystallinity. The structure of an individual alloy specimen results from random close packing of glassy-state atoms with nanocrystallites, as randomly selected from the ensemble of nanocrystallites having the designated size distribution for the particular given alloy composition. We note that the random assembly of the specimen is carried out in three dimensions. This means that a suitable procedure for transformation of the nanocrystallite size distribution in two dimensions into three dimensions must be established at some later stages of the theoretical development.

In order to model the thermal dissociation of a nanocrystallite in the alloy, we consider a nanocrystallite containing i-particles. We are interested in calculating the percentage of i-size crystallites that will thermally dissociate j times, losing j atoms from its surface. For each step of thermal dissociation, a nanocrystallite loses one atom from its surface, which then becomes part of the glassy matter. To lose j-atoms from the surface of a nanocrystallite would require j-reaction equations of thermal dissociation:

$$c_i \rightarrow c_{i-1} + A_g$$
$$c_{i-1} \rightarrow c_{i-2} + A_g$$
$$\vdots$$
$$c_{i-j+1} \rightarrow c_{i-j} + A_g$$
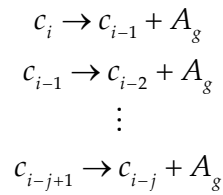
Here, c_i represents i-atom nanocrystallite and A_g the glassy-state atom as reactants. Each of these reactions may be expressed in the following form:

$$\sum_{i=reactant} v_i A_i = 0 \tag{1}$$

where A_i denotes i-th reactant and v_i is the number of i-th reactants that are needed to complete the reaction.

The assertion that only the atoms on the surface of the nanocrystallite undergo thermal dissociation is based on the fact that removal of a single atom from the surface would incur the lowest energy cost in the low temperature heating environment. A nanocrystallite breaking off chunks of atoms at a time would require much higher energy and therefore much less likely. With this system of reaction equations for each i-atom nanocrystallite, we have established the dissociation pathway along which each i-atom nanocrystallite becomes i atoms in the glassy matter medium.

The equation of state for the system of nanocrystallites and glassy state atoms can be expressed in the form of total volume occupied by all nanocrystallites and glassy state atoms. For instance, the thermal expansion of the specimen can be written out in terms of the alloy's thermal expansion coefficient of nanocrystallites ξ_c and of the glassy-state medium ξ_g:

$$V(N_0, T) = V_{C0}[1 + \xi_C(T - T_{rm})]^3 + V_{g0}[1 + \xi_g(T - T_{rm})]^3 \tag{2}$$

The equation of state depends on the system's state at room temperature. The alloy specimen will be constrained by the total number of atoms N_0, which is conserved:

$$N_0 = N_g + \sum_{i=2}^{i_{max}} D(R_i, T) N_i i \tag{3}$$

Here, N_g is the number of glassy-state atoms, $D(R_i, T)$ is the nanocrystallite size distribution, and N_i is the number of i-atom nanocrystallites in the specimen. The initial volume occupied by all nanocrystallites and the initial volume occupied by glassy-state atoms are, respectively,

$$V_{c0} = \sum_{i=1}^{i_{max}} D(R_i, T) \frac{4\pi R_i^{\,3}}{3} \tag{4}$$

$$V_{g0} = N_g \frac{4\pi R_g^{\,3}}{3} \tag{5}$$

where R_i is the nanocrystallite radius and R_g is the radius of the average volume needed for a single glassy-state atom. The morphology of the alloy specimen is represented by the degree of crystallinity, and the crystallite size distribution changes the individual parameters in each of these equations dictating the evolution of the alloy specimen as a function of temperature.

The chemical potential, i.e., the energy needed to increase the number of the i-th reactant species in the system by one, is found from the Gibbs free energy $F(T, p, N_1, N_2,...)$ of the system:

$$\mu_i = \frac{\partial F}{\partial N_i} = -k_B T \ln\left[q_i \,/\, N_i \right] \tag{6}$$

T is the specimen temperature, p the pressure and N_i the total number of i-th species within the specimen, either a nanocrystallite or a glassy state atom. k_B is the Boltzmann constant. q_i is the canonical partition function for the i-atom nanocrystallite. The reaction equilibrium satisfies the law of mass action, which may be written in the following form:

$$\prod_{i=reactant} \left[q_i \,/\, N_i \right]^{\nu_i} = 1 \tag{7}$$

There are (i-1) dissociation steps for an i-atom nanocrystallite. For each dissociation step, there is a reaction equation of the form of Eq. (1), and the corresponding law of mass action may be written in the following form:

$$\frac{q_i}{q_{i-1} q_A} = \frac{N_i}{N_{i-1} N_A} \tag{8}$$

We will later attend to the canonical partition function for each reactant in the reaction equation for thermal dissociation. In order to address the temperature dependence of the nanocrystallite populations by size we must solve the system of the law of mass action equations simultane-

ously. The dissociation of an atom from an i-atom nanocrystallite increases the population of $(i\text{-}1)$-atom nanocrystallites by one, which in turn affects the reaction equilibrium of the $(i\text{-}1)$-atom nanocrystallites with similar consequences on the populations of the smaller nanocrystallites. To help manage the simultaneous nature of the rather large number of reaction equilibria involved, we introduce the dimensionless degree of dissociation as follows:

$$\alpha_{i,j} = \frac{N_{i,i-1} + N_{i,i-2} + \cdots + N_{i,i-(j-1)}}{N_{i,i-1} + N_{i,i-2} + \cdots + N_{i,i-j}} \tag{9}$$

Here, $\alpha_{i,j}$ is defined as the ratio of the number of all initially i-atom nanocrystallites that have been dissociated once through j times to the number of all initially i-atom nanocrystallites that have been dissociated once through $(j-1)$ times. Since the distribution of nanocrystallites by size will be determined by the nanocrystallite size distribution at given atomic composition, each crystallite size will be populated at a certain number N_i. In order to track the evolution of the number of i-atom nanocrystallites as a function of temperature, we introduce the degree of dissociation. The degree of dissociation is the percentage of i-atom nanocrystallites that will dissociate j times. This expresses the remaining number of i-atom nanocrystallites after an increase in temperature, while also providing information on the size of the resulting nanocrystallites after the dissociation. In order to write the law of mass action equation in terms of the degree of dissociation, the number of i-atom nanocrystallites is replaced with the set of degrees of dissociation for the dissociation steps the nanocrystallites must undergo:

$$\frac{\left(1-\alpha_{i,j}\right)}{\alpha_{i,j}\left(1-\alpha_{i,j-1}\right)} = \frac{N_A q_{i-j}}{q_{i-j-1} q_A} \tag{10}$$

Let us consider, for example, dissociation of a 10-particle nanocrystallite. This will present nine stages of dissociation to consider and a set of nine coupled equations to calculate its degrees of dissociation, as shown below:

$$\frac{\left(1-\alpha_{10,1}\right)}{\alpha_{10,1}\left(1-\alpha_{10,2}\right)} = \frac{N_A q_9}{q_8 q_A}$$

$$\frac{\left(1-\alpha_{10,2}\right)}{\alpha_{10,2}\left(1-\alpha_{10,3}\right)} = \frac{N_A q_8}{q_7 q_A}$$

$$\vdots$$

$$\frac{\left(1-\alpha_{10,9}\right)}{\alpha_{10,9}} = \frac{N_A q_1}{q_2 q_A}$$

The structure of these coupled equations provides the method for computing the degrees of dissociation. It requires that the partition function for each nanocrystallite as well as the glassy state atoms in the alloy be known. Not only that these equations are coupled but also that each equation contains two undetermined degrees of dissociation. Each pair of successive equations shares a common degree of dissociation. An exception is that the last equation in the sequence of dissociation steps contains only one unknown degree of dissociation to be solved. It would seem possible to calculate the degree of dissociation in the last equation, if the right-hand side of the equation is fully prescribed. The solution may be carried into the next equation to solve for the remaining unknown degree of dissociation if its right-hand side is prescribed. This procedure can be continued for the full set of dissociation equations, provided that the total number of glassy-state atoms in the specimen at the given temperature is known.

The total number of glassy-state atoms is not known, however. At room temperature, the population of glassy state atoms in the alloy specimen is given by the degree of crystallinity. When significant thermal dissociation of nanocrystallites commences, N_A, the number of glassy state particles in the specimen, increases with temperature. The way the dissociation equations are presented above, N_A appears on the right-hand side of each equation so that the entire system of dissociation equations for the alloy specimen can be solved by the trial and error method. That is, first guess a value for $N_A^{(0)}$, solve for all $\alpha_{i,j}$'s and calculate $N_A^{(1)}$; continue until $N_A^{(l)}$ agrees with $N_A^{(l+1)}$ within a preset error. Here, l is an integer that tracks the number of iterations.

As nanocrystallites dissociate, the asymptotic value of $N_A^{(l)}$ will change as a function of temperature. This number of glassy-state atoms can then be recalculated using the set of degrees of dissociation and compared with the initial value to assess the self-consistency of the computation. If not in agreement within the preset error criterion, the process is reinitialized and computation is repeated until a satisfactory agreement is attained.

To calculate the coupled law of mass action equations, it is necessary to write the canonical partition functions for each of the reactants involved in the thermal dissociation reaction equation. The partition function of a reactant includes eigenstates according to all the degrees of freedom the reactant has, be it a nanocrystallite or a glassy state atom. However, we make a note of the fact that the canonical partition functions appear in each of the degrees of dissociation equations contains the partition functions in the form of the ratio of two partition functions—that is, the partition function of a nanocrystallite before, and after, a single-step dissociation. The partition function for a single i-particle nanocrystallite may be written out as follows:

$$q_i = \left(q_{trans} q_{rot} q_{vib} \right)_i$$

or,

$$\frac{q_{i-j}}{q_{i-j-1}} = \left(\frac{q_{i-j}}{q_{i-j-1}}\right)_{trans} \left(\frac{q_{i-j}}{q_{i-j-1}}\right)_{rot} \left(\frac{q_{i-j}}{q_{i-j-1}}\right)_{vib}$$

The subscripts *trans*, *rot*, and *vib* denote, respectively, translational, rotational, and vibrational degrees of freedom. The rotational and vibrational motions of the nanocrystallites are dominated by the crystalline structure, and we approximate the ratio to be unity to find:

$$\frac{q_{i-j}}{q_{i-j-1}} \approx \left(\frac{q_{i-j}}{q_{i-j-1}}\right)_{trans}$$

The translational degrees of freedom give rise to the partition function of *i*-particle nanocrystallite at temperature *T* as follows:

$$\left(q_{trans}\right)_i = V\left(\frac{2\pi i M k_B T}{h^2}\right)^{3/2} \tag{11}$$

V is the volume of the alloy specimen, *m* is the mass of the atom in the glassy matter, *T* is the temperature of the specimen, k_B is Boltzmann's constant, and *h* is Planck's constant. Thus, we write Eq. (11) as follows:

$$\frac{\left(1-\alpha_{i,j}\right)}{\alpha_{i,j}\left(1-\alpha_{i,j-1}\right)} = \frac{N_A}{V}\left(\frac{i-j+1}{i-j}\right)^{3/2}\left(\frac{2\pi M k_B T}{h^2}\right)^{-3/2}\exp\left(\frac{D_{i-j+1}}{k_B T}\right) \tag{12}$$

where *M* denotes atomic mass. In the event that the specimen is a binary alloy of given composition, *M* would be the average atomic mass, weighted at the alloy composition. D_{i-j+1} is the dissociation potential for a particle on the periphery of the (*i*–*j*) particle nanocrystallite. It measures the zero of the energy scale of the nanocrystallite after the dissociation of a single particle relative to that of the nanocrystallite before dissociation. In other words, it is the energy needed to remove an atom from the surface of the (*i*–*j*+1) atom nanocrystallite by thermal dissociation.

6. Calculation of the dissociation potential

The most important part of the law of mass action computation is the energy of thermal dissociation or the dissociation potential. A particle on the surface of a nanocrystallite is bound to the surface an attractive potential, and it must overcome this potential energy to be dissociated from the surface to become a glassy state atom.

The final key parameter needed for calculation of the series of law of mass action equations is the potential energy experienced by an atom on the surface of an i-atom nanocrystallite or the dissociation potential $D_{0,\,i}$. For each nanocrystallite of the alloy, we calculate this potential according to the unit cell information for the alloy specimen as a single crystal and the Lennard-Jones parameters for the interacting atom pairs contained in the nanocrystallite of the alloy. Our first approximation is to treat each i-atom nanocrystallite to be spherical in shape. Using the structural information for the alloy as a single crystal, we begin with a cubic sample of the crystalline alloy and sculpt a spherical nanocrystallite of radius r by chiseling away atoms farther than a radius r from the center of the sample. In this manner, the full set of spherical nanocrystallites, as specified by the nanocrystallite size distribution function for the alloy, is generated.

The surface atoms in each of these spherical nanocrystallites are considered in the determination of the dissociation potential. To find the dissociation potential, we must take sum of all of the interatomic interaction potential contributions from every other atom in the nanocrystallite. Using the Lennard-Jones potential, we write the interaction potential for i-th atom due to N-atom nanocrystallite as follows:

$$V_i = \sum_{j=1}^{N} 4\varepsilon_j \left[\left(\frac{\sigma_j}{r_{ij}} \right)^{12} - \left(\frac{\sigma_j}{r_{ij}} \right)^{6} \right] \tag{13}$$

For most of the metallic elements, Lennard-Jones potential constants σ_j and ε_j have already been computed through quantum chemistry calculations [20]. In a binary nanocrystallite, these quantum chemistry values cover only the like atom interactions. To account for potential interactions between unlike atoms, as indicated by i and j that are unequal, we make use of the Kong combination rules for Lennard-Jones potential parameters [21]:

$$\epsilon_{ij}\sigma_{ij}^{\;6} = \left(\epsilon_{ii}\sigma_{ii}^{\;6} \epsilon_{jj}\sigma_{jj}^{\;6} \right)^{\frac{1}{2}} \tag{14}$$

$$\epsilon_{ij}\sigma_{ij}^{\;12} = \frac{\epsilon_{ii}\sigma_{ii}^{\;12}}{2^{13}} \left[1 + \left(\frac{\epsilon_{jj}\sigma_{jj}^{\;12}}{\epsilon_{ii}\sigma_{ii}^{\;12}} \right)^{\frac{1}{13}} \right]^{13} \tag{15}$$

As illustrated in **Figure 6** to calculate the total interaction potential, we move the surface atom radially outward from the center of the nanocrystallite and calculate the total interaction potential at each radial position. We repeat this calculation for all of the surface atoms and take an average over all of the surface atoms. For a binary nanocrystallite, there are different dissociation potentials for different atom pairs. The dissociation potential is calculated for all

of the three possible pairs of atoms, but the final value of the dissociation potential is assigned with the weighted average of the two atom types according to atomic composition of the binary alloy specimen. Nanocrystallites of different sizes are built and analyzed in the similar manner.
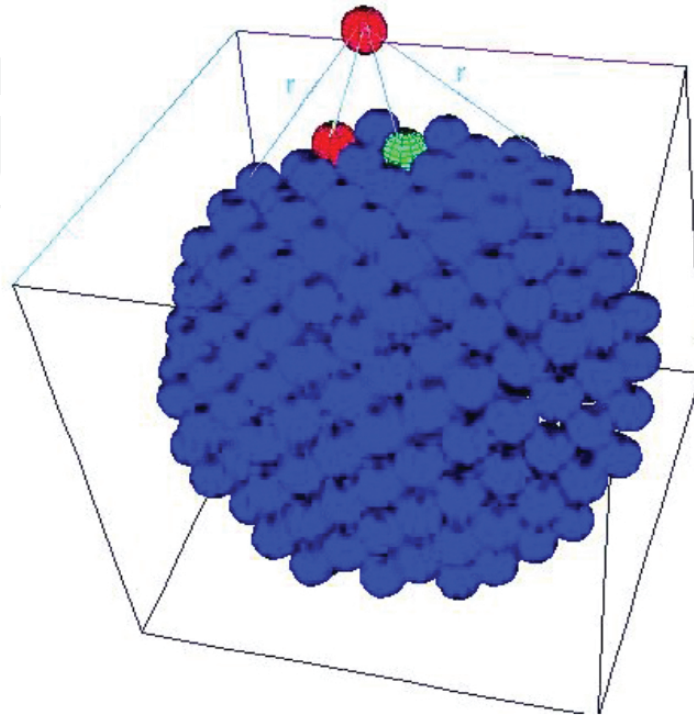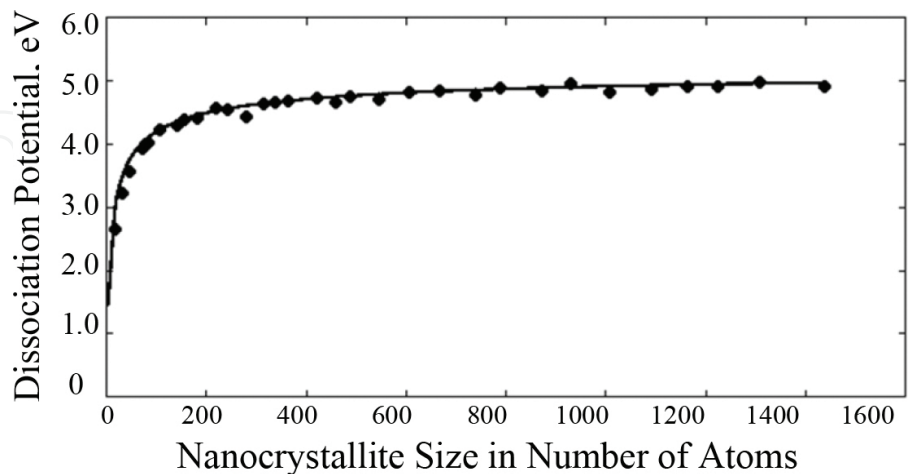

Figure 6. The dissociation potential for a single particle on the surface of a nanocrystallite is the energy needed to free a surface atom against attraction by all atoms in the nanocrystallite. The work done to move the atom in red to infinity is computed. The computation is repeated for all possible surface positions and pairings of surface atoms with the rest of the atoms within the nanocrystallite

For the alloy of $AuCu_3$ computation, we have used $\sigma_j = 2.6367 \times 10^{-10}$ m and $\varepsilon = 5152.9$ K for gold and $\sigma_j = 2.3374 \times 10^{-10}$ m and $\varepsilon = 4733.5$ K for copper [20]. The computed dissociation potential grows with increasing size of the nanocrystallite as shown in **Figure 7**, and this can be fitted by an analytical function. The resulting dissociation potential function can then be incorporated into the system of simultaneous algebraic equations for the large number of degrees of dissociation needed in the law of mass action reaction equilibrium computation. The dissociation potential grows to an asymptotic value for large nanocrystallites. To fit the dissociation potential as a function of nanocrystallite size, it is necessary to look at how the dissociation potential differs from the asymptotic value. When the values of the dissociation potential are subtracted from the asymptotic value and plotted on a log-log scale, a linear relation between the dissociation potential and nanocrystallite size is seen. To get the best fit possible for this functional dependence, a constant is added to optimize the fit. This fit has the functional form of

$$D(i) = D(Large\, i\, limit) - A * i^B + Constant \tag{16}$$

An example of the fitting procedure for the alloy $AuCu_3$ can be seen in **Figures 7** and **8**. **Figure 8** shows a straight-line fit of the computed dissociation energy as a function of nanocrystallite size in number of particles that are contained in each crystallite.

Figure 7. Energy required for removal of a single surface atom from a nanocrystallite by thermal dissociation as a function of nanocrystallite size for the $AuCu_3$ alloy.
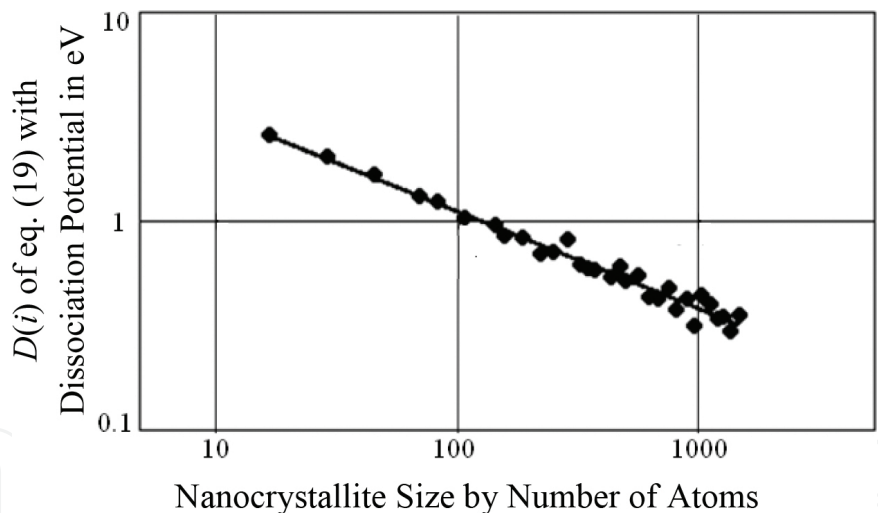

Figure 8. The computed dissociation potential of **Figure 7** as a function of nanocrystallite size is transformed into $D(i)$ of Eq. (9), and $D(i)$ is plotted as a straight line against nanocrystallite size for the $AuCu_3$ alloy.

7. Theoretical prediction of disorder in $AuCu_3$ at elevated temperatures

We consider the case of the binary alloy, $AuCu_3$, which has an alloy composition of 75% copper (small) to 25% gold (large) with the respective atomic radii of gold and copper. The structure of the alloy is known based on the 3D nanocrystallite size distribution. In order to determine

the number of atoms contained in each nanocrystallite size bin, we need to know the total number of atoms in the alloy specimen to be modeled. Using $AuCu_3$ as an example again, we have the atomic mass of each of the two different atoms in the alloy: $m_{Cu} = 6.655 \times 10^{-23}g$ and $m_{Au} = 3.27 \times 10^{-22}g$. From the mass density, we know the relationship between the number of particles in the alloy specimen and the volume of the specimen, where the mass density of the alloy $\rho_{AuCu_3} = 10.9946$ g/cm^3 ($AuCu_3$ parameters are obtained from reference [22]).
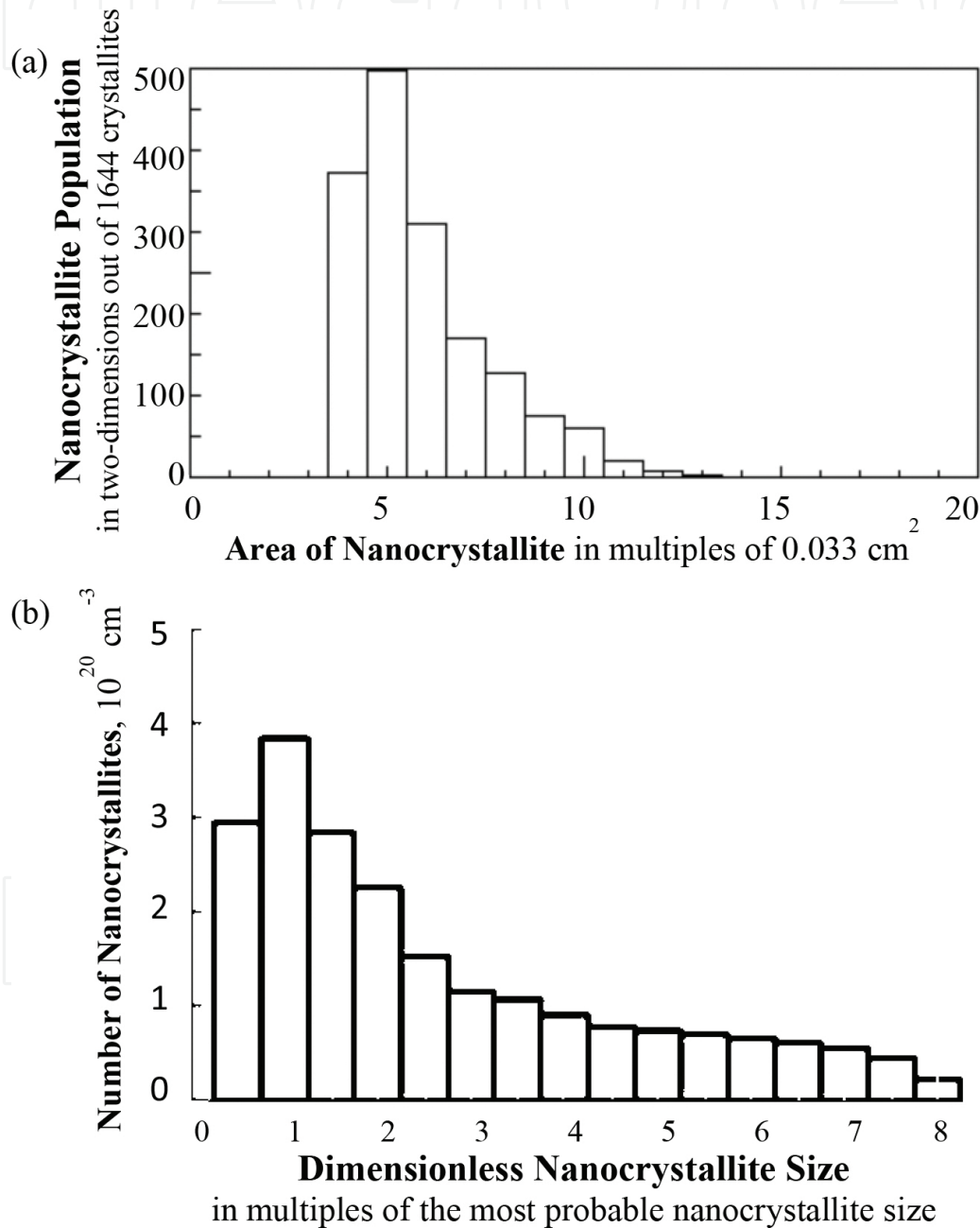
Figure 9. Nanocrystallite size distribution for alloy $AuCu_3$ at room temperature. The measured distribution function at alloy composition of 25W%Au:75W%Cu in two dimensions is shown in (a). The distribution after the transformation into three dimensions is shown in (b).
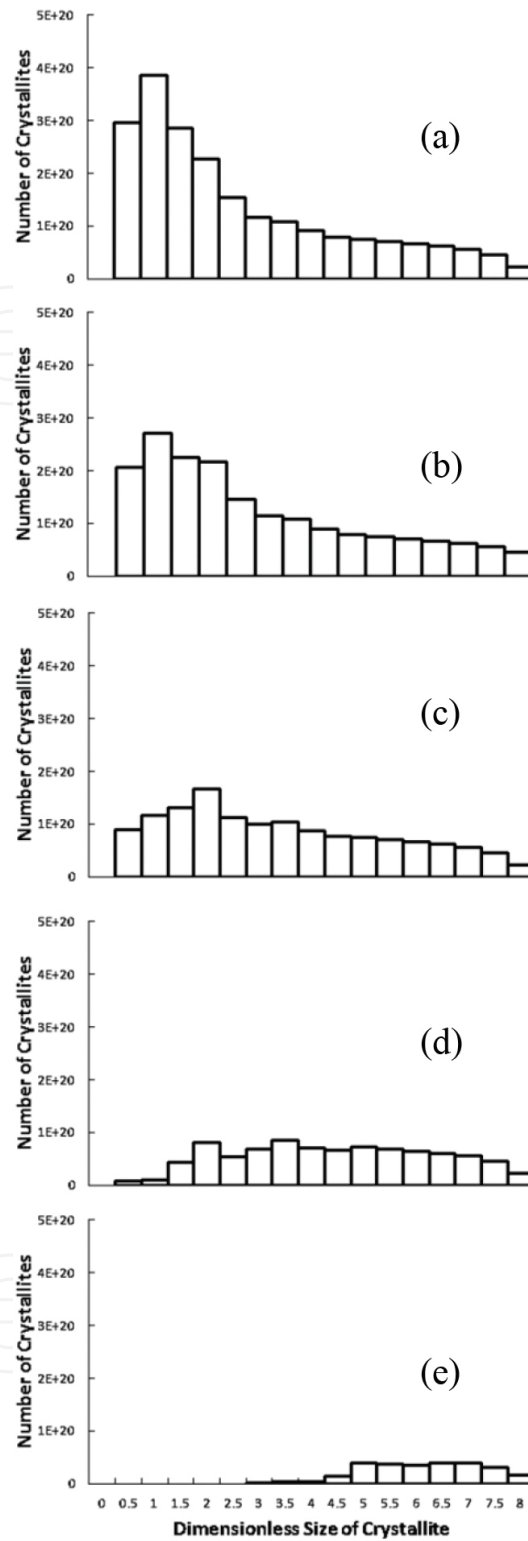
The initial nanocrystallite size distribution for alloy $AuCu_3$ is needed to carry out the law of mass action equation calculations for the degrees of dissociation at elevated temperature, and we make use of the measurement from the simulated alloy medium in two dimensions. The size of the nanocrystallite is represented in our modeling in terms of the area of a circle, and therefore the corresponding size of the nanocrystallite in three dimensions would be given by the volume of a sphere having the same radius of the circle in two dimensions. The 2D size distribution is transformed to three dimensions according to the reasoning that the size of a nanocrystallite in three dimensions would scale as the size in 2D raised to 3/2 power. Both the nanocrystallite size distribution in 2D and in 3D are shown in **Figure 9**.

In order to explore the morphology of the alloy as a function of the specimen temperature, it is necessary to carry out the law of mass action calculation at each given temperature to determine how the structure of the specimen evolves as a function of temperature. The value that is calculated through the set of equations is the degrees of dissociation or the amount of nanocrystallites of a certain size changing due to dissociation. Each numerical value of the degree of dissociation that is above zero means a thermal dissociation reaction for the nanocrystallite of particular size. The result of any such reaction means a change in the nanocrystallite size distribution as well as a change in the total number of atoms in the glassy state matter. The population at each nanocrystallite size is adjusted after the full set of degrees of dissociation values has been calculated. The number of i-sized nanocrystallites is adjusted according to the formula below:

$$N_i = N_{i0}(1 - \alpha_{i,1}) + \sum_{j>i}^{j=max} N_j(1 - \alpha_{j,j-i+1}) \left(\prod_{k=1}^{k=j-i} \alpha_{j,k} \right) \tag{17}$$

N_{i0} is the initial number of i-sized nanocrystallites before the temperature has been raised. The first term in the formula accounts for any of the nanocrystallites that are lost out of the group due to dissociation, which will in turn reduce the number of the nanocrystallites of the particular size. The second term in the formula accounts for larger nanocrystallites that would become i-atom nanocrystallites after going through stages of dissociation. This term accounts for an increase in the number of i-sized crystallites.

Figure 10 displays the result from calculations of the degrees of dissociation for a series of temperatures for the alloy AuCu$_3$. As can be seen, the crystallite size distribution evolves as the temperature is raised, and **Figure 10** shows how the populations of nanocrystallites of different sizes are affected by the temperature change. As the nanocrystallites dissociate, the total number of atoms tied up in nanocrystallites decreases, and this causes a change in the degree of crystallinity. The numerical value of the degree of crystallinity at each temperature step is shown in the caption of **Figure 10**.

Figure 10. The nanocrystallite size distribution of the $AuCu_3$ alloy at elevated temperatures is computed using the law of mass action reaction equilibrium equations. Thermal dissociation of the distribution of nanocrystallites at room temperature is carried forward as the alloy temperature is increased. The vertical axis displays the number of nanocrystallites per cm^3. The temperature and the computed degree of crystallinity of each graph are as follows: (a) 300 K, γ =0.316; (b) 1000 K, $\gamma = 0.306$; (c) 1100 K, $\gamma = 0.276$; (d) 1200 K, $\gamma = 0.203$; and (e) 1400 K, $\gamma = 0.051$.

As the nanocrystallites in the alloy specimen undergo thermal dissociation, the number of glassy state atoms increases due to changing degrees of dissociation as follows:

$$N_A = N_{A0} + \sum_{i=2}^{i=max} N_{i0} \prod_{j=1}^{j=i-1} \alpha_{i,j} + \sum_{i=2}^{i=max} (N_i - N_{i0}) \tag{18}$$

N_{A0} is the number of glassy state atoms prior to heating, and there will be no decrease in the number because we are concerned with increases in temperature. The second term accounts for all of the fully dissociated nanocrystallites. The third term accounts for all glassy state atoms from partial dissociation reactions associated with each temperature rise. Note that with each thermal dissociation event, an atom is added into the ranks of glassy state matter.

Figure 11 shows the number of glassy state atoms in the alloy specimen as a function of temperature for the alloy AuCu$_3$. The vertical broken line inserted in the figure shows the known melting point of this particular alloy. As can be seen, the approximate model of the disordered alloy specimen not only reveals a well-behaved functional form of thermal dissociation of nanocrystallites in the alloy as the temperature is increased but also provides an effective physical mechanism for identifying the melting temperature of the alloy. A definition of the melting point could be the temperature at which one half of all nanocrystallite atoms within the alloy at room temperature are dissociated into glassy state atoms. Another definition is possible based on the temperature at which the thermal dissociation rate maximizes; this may provide a way to fine tune the melting point.
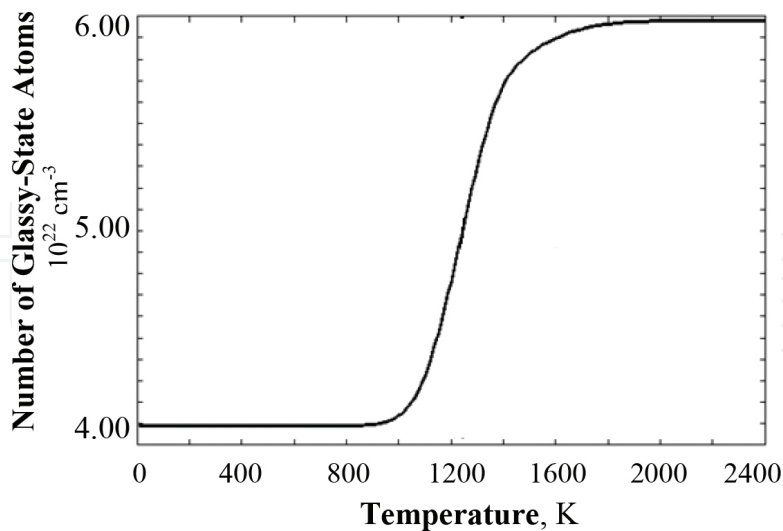
Figure 11. Number of glassy state atoms as a function of temperature in alloy AuCu$_3$. The dashed line shows the known melting temperature of 1240 K of the alloy in excellent agreement.

This technique was used to predict the melting temperature for a number of metallic elements and a group of six binary alloys. The results from the lowest order approximation of the

disorder in metallic alloys, as described above, are summarized in **Tables 1** and **2**. The good agreement of the computed melting points of the high temperature metals and alloys with the known experimental melting point values presents considerable confidence in the validity of our approach. The limited number of binary alloy calculations is due to the lack of available unit cell structure information for binary alloys, which is necessary for execution of our disorder modeling approach.

Element	Symbol	σ (Å)	ε (eV K)	Lattice constant (Å) [21]	Known melting point, K [21]	Predicted melting point (@ 50% dissociation), K
Rhodium	Rh	2.4622	0.6699	3.8	2233	2360
Iridium	Ir	2.4839	0.8077	3.84	2716	2730
Tantalum	Ta	2.6819	0.9809	3.31	3269	2905
Chromium	Cr	2.3357	0.4988	2.88	2163	2245
Tungsten	W	2.5618	1.0644	3.16	3653	3840
Hafnium	Hf	2.8917	0.750989	3.2	2423	2160
Ruthenium	Ru	2.4447	0.788343	2.7	2523	2410
Titanium	Ti	2.6841	0.568102	2.95	1948	1900
Zirconium	Zr	2.9318	0.738442	3.232	2125	2230

Table 1. Refractory metallic elements.

Alloy [22–26]	Lattice constant, Å	Known melting point, K	Predicted melting point (@ 50% dissociation), K
$AuCu_3$	3.74	1240.5	1320
AuCu	3.964 (2), 3.672	1183	1410
Au_3Cu	3.964	1151.5	1495
Al_3Ti	3.964	1340	1260
AlTi	4.00 (2), 4.075	1729	1935
$AlTi_3$	a =5.780, c=4.674	1473	1360

Table 2. Binary alloys.

8. Concluding remarks

The modeling technique presented above provides a first principle approach to modeling the morphology of a disordered binary alloy under a variety of equilibrium thermal forcing conditions. The success in predicting the accepted melting temperatures of the metallic elements and binary alloys demonstrates that the approximations made in the coarse-grained

assessment of disorder in binary alloys are reasonable and by and large correct. By the same token, we note that there are many opportunities for improving the outcomes of the disordered alloy modeling.

The framework for modeling the morphology of disordered metallic binary alloys has been built on the basis of a randomly close-packed assembly of constituent atoms. The RCP structure is treated as a mixture of nanocrystallites and glassy state matter. The fraction of all atoms tied up in crystalline structures defines the degree of crystallinity. The distribution of nanocrystallites at given size of the structure has been measured in the form of the crystallite size distribution function in two dimensions. Both of these characterizations are found to be dependent on alloy composition. The histogram of the nanocrystallite size distribution provides the snapshot of the equilibrium structure of the alloy at room temperature when transformed into three dimensions. Our theoretical modeling takes off from the 2D RCP media in two dimensions at six different compositions. The morphological alloy data have been obtained from the simulated alloys by experiment, which have also provided the realistic measures of the degree of crystallinity.

The evolution of the morphology in a disordered alloy specimen is modeled as the case of thermal dissociation of nanocrystallites within the alloy specimen by means of the law of mass action. The theoretical model begins with the room temperature structure of the alloy specimen as summarized above. We assumed it to be a randomly close-packed medium of nanocrystallites and glassy state atoms. The temperature-dependent evolution of the size distribution of the nanocrystallites within an alloy specimen is treated as the case of reaction equilibrium according to the law of mass action, as imposed on each stage of dissociation of all nanocrystallites within the alloy specimen. The very large system of coupled law of mass action equations is solved for each possible dissociation step of the nanocrystallites of the specimen. To facilitate the computational procedure, we have introduced a set of degrees of dissociation, each as a measure of the fraction of nanocrystallites at given size that dissociate into smaller nanocrystallites while increasing the population of glassy-state atoms, at given temperature. Various alloy parameters are important in the calculation of each degree of dissociation equation, but the main determining parameter for the temperature at which dissociation happens is the dissociation potential, i.e., the energy needed to extract individual atoms from the surface of each nanocrystallite of given size. This quantity is calculated for an atom on the surface of a spherical crystallite of given size. The energy is found by considering all interactions with all other atoms of the nanocrystallite. This potential was calculated assuming interatomic interactions of the Lennard-Jones type. We have made use of the Lennard-Jones parameters that have been obtained by the method of quantum chemistry computation for the pairs of like atoms in the alloy [20]; for interactions between two dissimilar atoms, the Kong combination rules are used [21].

The success of the model is demonstrated by the accurate prediction of the melting temperatures for disordered high-temperature refractory metals as well as for some binary alloy specimens. The morphology of the disordered alloy structure can now be predicted analytically at arbitrarily high temperatures. This makes it possible to predict the thermal transport properties for disordered alloys as a function of temperature. The important features of the

alloy structure that pertain to calculation of thermal conductivity at elevated temperatures are the structure of the nanocrystallites as specified in terms of the nanocrystallite size distribution, the density of glassy state matter, and the interfaces between them. All necessary details of the structure become available from the computed solutions of the system of the law of mass action equations as applied to the specifics of the initial state of the alloy by means of the nanocrystallite size distribution function.

We have shown the full modeling sequences for thermal forcing of disordered binary alloys. The method is sufficiently general for applications to forcing of alloys by mechanical stress, neutron bombardment, or chemical reactions. Our modeling approach may also be fine-tuned for improved accuracy by adding more refined microscopic details that are specific to a given alloy system. For example, the spherical shape used for all nanocrystallites may be relaxed to allow for elliptical or rectangular shapes with variable aspect ratio or to highlight the prevailing crystalline symmetry properties of particular alloy composition. There are many other possibilities. We may broaden the modeling to include characterization of tertiary or even more complex alloys. Ultimately, it appears quite remarkable that one may effectively characterize the morphology of many disordered metallic alloys as a fluid-like mixture of nanocrystallites and glassy state atoms.

Author details

Ryan P. Cress and Yong W. Kim[*]

[*]Address all correspondence to: ywk0@lehigh.edu

Department of Physics, Lehigh University, Bethlehem, Pennsylvania, USA

References

[1] Kim, Y.W., "Routes to Development of Near-Surface Alloy Composition Anomaly," International Journal of Thermophysics 26, (2005): 1051.

[2] Kim, Y.W., "Development of Transport Property-Composition Relationship by Thermal Modification of Alloy Composition Profile," High Temperatures - High Pressures 38, (2009): 1.

[3] Kim, Y.W., "Surface Position-Resolved Thermophysical Properties for Metallic Alloys," International Journal of Thermophysics 28, (2007): 732.

[4] Kim, Y.W., "Simultaneous Multitemperature Measurements of Thermal Diffusivity and Composition," International Journal of Thermophysics 31, (2010): 926.

[5] Kim, Y.W. and R.P. Cress, "Effects of Thermal Forcing on Morphology of Disordered Binary Metallic Alloys: Local Equilibration and Modification of Near-Surface Elemental Composition," High Temperature – High Pressure 40, (2011): 335.

[6] Ho, C. Y., M. W. Ackerman, K. Y. Wu, S. G. Oh, and T. N. Havill. "Thermal Conductivity of Ten Selected Binary Alloy Systems," Journal of Physical and Chemical Reference Data 7, 3 (1978): 959.

[7] Van Swygenhoven, H., and J. Weertman. "Deformation in Nanocrystalline Metals," Materials Today 9, 5 (2006): 24-31.

[8] Tongjai, C., H. A. Murdoch, and C. A. Schuh. "Design of Stable Nanocrystalline Alloys," Science 337, 6097 (2012): 951-54.

[9] Barker, J. A., M. R. Hoare, and J. L. Finney. "Relaxation of the Bernal Model," Nature 257, (1975): 120.

[10] W. O. Smith, P. D. Foote, and P. F. Busang, Physical Review 34, (1929): 1271.

[11] J. D. Bernal, Proceedings of the Royal Society London A280, (1964): 299.

[12] C. H. Bennett, Journal of Applied Physics 43, (1972): 2727.

[13] C. A. Rogers, Packing and Covering, Cambridge University Press, 1964).

[14] J. L. Finney, Proceedings of the Royal Society of London A319, (1970): 479.

[15] G. D. Scott and D. M. Kilgour, British Journal of Applied Physics (Journal of Physics D) 2, (1969): 863.

[16] Berryman, J. G. "Random Close Packing of Hard Spheres and Disks." Physical Review A27, (1983): 1053.

[17] Rintoul, M. D., and S. Torquato, "Hard-sphere Statistics along the Metastable Amorphous Branch." Physical Review A58, (1998): 532.

[18] Anikeenko, A. V., and N. N. Medvedev, "Structural and Entropic Insights into the Nature of the Random-Close-Packing Limit," Physical Review E77, (2008): 031101.

[19] L.D. Landau and E.M. Lifshitz, Statistical Physics, Elsevier, 1980).

[20] S. Zhen and G. J. Davies, "Calculation of the Lennard-Jones N-m Potential Energy Parameters for Metals," Physica Status Solidi 78, (1983): 595.

[21] Kong, C. L., "Combining Rules for Intermolecular Potential Parameters. II. Rules for the Lennard-Jones (12–6) Potential and the Morse Potential," The Journal of Chemical Physics 59.5 (1973): 2464.

[22] Han, X. J., M. Chen, and Z. Y. Guo, "Thermophysical Properties of Undercooled Liquid Au–Cu Alloys from Molecular Dynamics Simulations," Journal of Physics: Condensed Matter 16, 6 (2004): 705-13.

[23] Lide, D. R., CRC Handbook of Chemistry and Physics, CRC Press, 1994)

[24] Okamoto, H., D. J. Chakrabarti, D. E. Laughlin, and T. B. Massalski, "The Au−Cu (Gold-Copper) System," Journal of Phase Equilibria 8, 5 (1987): 454-74.

[25] Batalu, D., G. Cosmeleata, and A. Aloman, "Critical Analysis of the Ti-Al Phase Diagrams." UPB Scientific Bulletin. B68.4 (2006).

[26] Djanarthany, S., J. C. Viala, and J. Bouix, "An Overview of Monolithic Titanium Aluminides Based on Ti_3Al and TiAl," Materials Chemistry and Physics 72, 3 (2001): 301-19.